Lightweight rotor design by optimal spar cap offset

2016 J. Phys.: Conf. Ser. 753 062003

(http://iopscience.iop.org/1742-6596/753/6/062003)

Lightweight rotor design by optimal spar cap offset

A Croce[1], L Sartori[1], M S Lunghini[1], L Clozza[1], P Bortolotti[2] and C L Bottasso[1,2]

[1] Department of Aerospace Science and Technology, Politecnico di Milano, Milano, Italy
[2] Wind Energy Institute, Technische Universität München, Garching, Germany

E-mail: alessandro.croce@polimi.it

Abstract. Bend-twist coupling behavior is induced in a blade by displacing the suction side spar cap towards the leading edge, and the pressure side one in the opposite direction. Additional couplings are introduced by rotating the spar cap fibers. The structural configuration of the blade is optimized using an automated design environment. The resulting blade shows significant benefits in terms of mass and loads when compared to the baseline uncoupled one. Finally, the lightweight design concept is used to increase the rotor size, resulting in a larger energy yield for the same hub loads.

1. Introduction

In large wind turbines, specific aero-structural solutions can be adopted for passive load mitigation, for example by tailoring the structure in order to couple the bending and twisting (bend-twist coupling, BTC) of the blade (cf. for example [1] and references therein). Recently Buckney et al. [2, 3, 4] have shown how a chord-wise misalignment of the spar caps may increase the structural efficiency of the blade. However, their preliminarily results were obtained throughout a topological optimization in a simplified design environment with frozen loads, and for rotors of different diameter. More recently, within the European project INNWIND.EU, Tibaldi et al. [5] have presented a two-bladed design concept introducing a spar cap offset. In this case the authors have included a forward offset of both the upper and lower spar caps with respect to the main axis and have not considered fatigue loads in the design process. In the present work, starting from the topological solutions presented by Buckney et al., we extend this approach by investigating in detail the effects of a parametric offset between the pressure-side and suction-side spar caps within the multi-level design suite `Cp-Max` [6]. This way, each design is obtained by the solution of a mass-minimizing optimization procedure, in which the driving ultimate and fatigue loads are recursively re-computed.

A detailed analysis of the results shows how the beneficial effects of a uniform spar offset are due to an enhanced flap/edge coupling, which induces the blade to sweep backward under loading. In order to maximize the benefits of this solution, at first an optimal offset is identified that offers the best performance in terms of mass and load reduction. Then, the corresponding solution is further investigated by applying a varying amount of fiber rotation in the two spar caps, showing that significant benefits in terms of loads and mass reduction could be achieved by exploiting the synergy of the two techniques. Since the main drawback of this lightweight design process is a significant loss in AEP, a final step is performed in which the rotor radius

is gradually increased in order to exploit the reduced loads to improve the energy yield of the wind turbine, thus obtaining a net reduction in the cost of energy.

2. Approach and methods

Analyses are carried out on a 10 MW reference wind turbine, whose structural components were preliminary optimized within the INNWIND.EU project [7, 8]. The original blade has two identical and straight spar caps of constant width, made of E-glass unidirectional plies, mainly sized by the stiffness requirements for the first flapwise frequency to be higher than 3P and maximum tip deflection. Within `Cp-Max`, loads are computed at each iteration from a set of relevant DLCs including 1.1, 1.3, 2.1, 2.3, 6.1, 6.2 and 6.3 [9]. All simulations are automatically managed by the multi-body aeroelastic code `Cp-Lambda` [11], so that all the physical phenomena and aero-structural couplings occurring during the dynamic load cases can be taken into account for the purpose of optimizing the various structural elements.

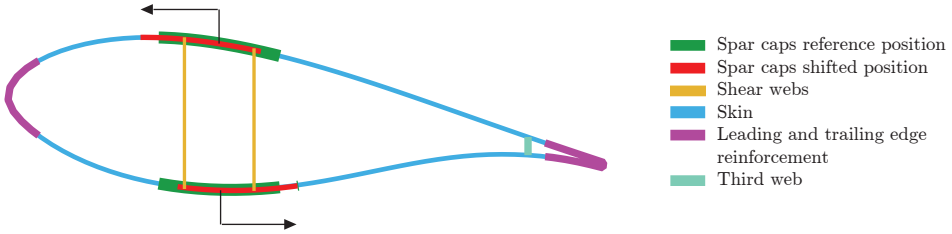

Figure 1: Sectional topology and positive offset definition.

Table 1: Structural design variables.

Element	Material	Number of spanwise design variables
Shell	Texture	16
Spar Caps	Unidirectional	16
Shear Webs	Biaxial	16
LE Reinforcements	Unidirectional	11
TE Reinforcements	Unidirectional	11
Root Reinforcement	Unidirectional	9
Third Web	Texture	10

Table 2: Structural constraints.

First blade flapwise frequency higher than 3P
First blade edgewise frequency higher than first flapwise
Maximum blade tip displacement lower than blade/tower clearance
Resistance to fatigue loads
Ultimate stress and strain lower than admittables

Starting from the baseline configuration [8], an offset is introduced by shifting the spar caps from their reference position. As illustrated in Figure 1, a positive offset implies that the suction-side spar cap is moved towards the leading edge, while the pressure-side spar cap is moved in the opposite direction. Both are displaced by a constant amount along the entire blade span. Parametric analyses are performed by gradually increasing the shift of the spar caps. For each configuration, a complete structural optimization is performed by `Cp-Max` in which the thickness of all the structural components are designed iteratively until a mass-minimizing solution is found. This way, each parametric solution is intrinsically feasible and satisfies all the design requirements in terms of stiffness, strength and resistance to fatigue.

In this work we consider blade shells manufactured in two halves from infused triaxial E-glass material, each incorporating a single spar cap made primarily of unidirectional material. Finally the two straight shear webs are infused separately and bonded between the shells. Starting from these manufacturing constraints, the maximum theoretical shift of the spar caps is determined by the requirement that both shear webs must be contained within the spar cap width. Table 1 shows a brief summary of the structural components of the blade, and the corresponding number of spanwise design variables considered during the design process. Table 2 lists the main constraints that are taken into account during the structural design.

3. Results

3.1. Optimal spar cap offset

A first study was performed by comparing the baseline against three different solutions obtained respectively for a uniform positive offset of 10, 20 and 30 cm. Figure 2 and Figure 3 show that an offset of 20 cm is the most beneficial one, leading to a mass decrease of 4% and a reduction of 10% in the hub and tower top combined moments.

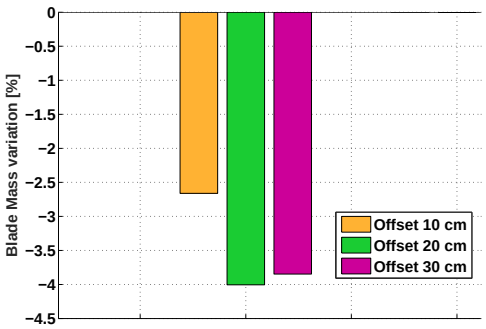

Figure 2: Blade mass variation.

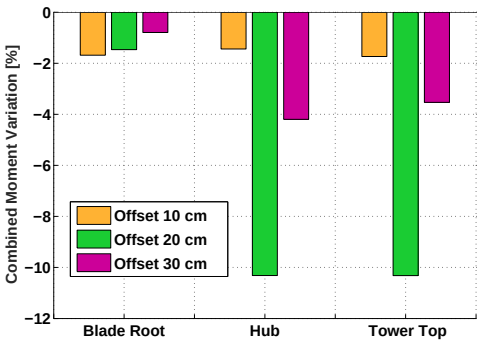

Figure 3: Ultimate loads variation.

Aeroelastic analyses under gust and static load conditions show that the the load reduction is due to an increased coupling between out- and in-plane bending. In these configurations, compressive/extensive forces arising in the spar caps during out-of-plane bending induce in-plane deformations. In turn, in-plane bending creates a backward sweeping effect. As a swept-back blade is characterized by a kinematic coupling between out-of-plane bending and twisting, the resulting nose-into-the-wind rotation of the blade sections induces a reduction in angle of attack that is finally responsible for the load decrease. This phenomenon can be quantified by introducing a non-dimensional coupling coefficient α_{FE}, which is conceptually similar to the one

Table 3: Blade mass and ultimate loads for the parametric offset.

	Baseline	Offset 10 cm	Offset 20 cm	Offset 30 cm
Blade mass [kg]	42445	41310 (-2.7%)	40741 (-4.0%)	40803 (-3.9%)
Blade root comb. mom. [kNm]	72497	71276 (-1.7%)	71435 (-1.5%)	71922 (-0.8%)
Hub comb. mom. [kNm]	60334	59465 (-1.4%)	54109 (-10%)	57803 (-4.2%)
Tower top comb. mom. [kNm]	62012	60937 (-1.7%)	55613 (-10%)	59823 (-3.5%)

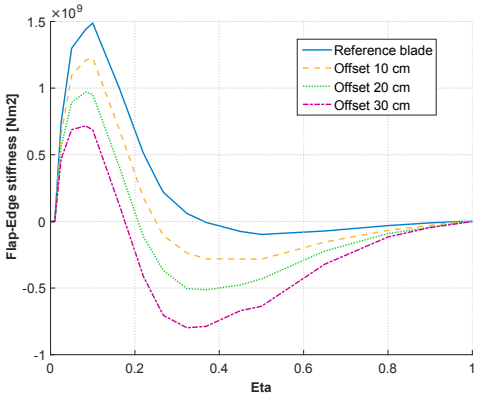

Figure 4: Flap/edge coupling stiffness distribution.

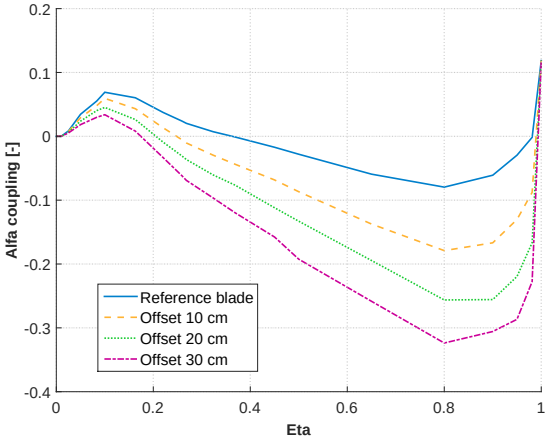

Figure 5: Flap/edge coupling coefficient α_{FE}.

employed for the BTC case (cf. [1] and references therein), and that can be defined as follows:

$$\alpha_{FE} = \frac{(K_{Flap\_Edge})^2}{\sqrt{K_{Flap} \cdot K_{Edge}}} \tag{1}$$

Figure 4 shows the extra-diagonal term of the stiffness matrix associated to the flap/edge coupling, while Figure 5 shows the coefficient α_{FE} along the blade span. Both suggest that a dependency exists between the flap/edge coupling and the amount of offset introduced between the spar caps, so that an increasing offset results globally in a stronger coupling. In the geometric description of the blade, a negative value of the flap/edge coupling term implies that a positive flapwise moment from the pressure to the suction side results into a backward deflection. The resulting BTC behavior is conceptually similar, although due to a completely different mechanism, to the one obtained by changing the fiber orientation in the spar caps.

3.2. Optimal offset and fiber orientation

For the blade under investigation, it was previously proven that inducing some BTC in the blade response through a carefully tuned rotation of the spar cap fibers could result in significant advantages in terms of mass and loads [4]. Here, in order to evaluate if this technique can work in synergy with the flap/edge coupling induced by the spar cap offset, the optimal blade with 20 cm offset of the previous study was modified by applying a parametric rotation to the fibers of the two spar caps.

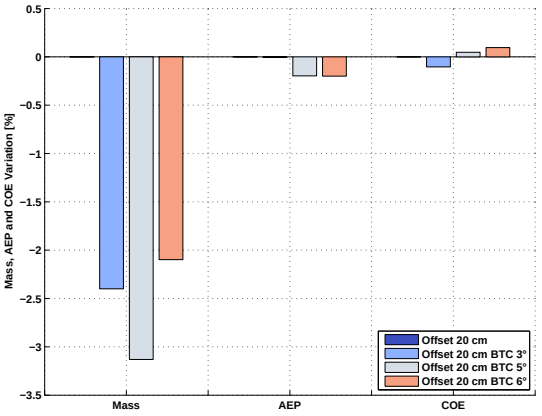

Figure 6: Parametric fiber rotation: mass, AEP and COE.

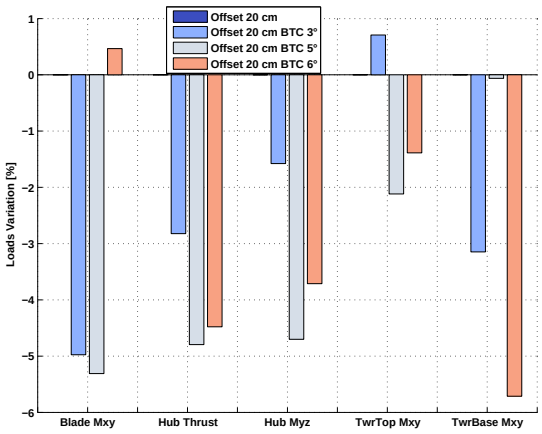

Figure 7: Parametric fiber rotation: ultimate loads.

Figure 6 and 7 show the key performance of the parametric solutions, with respect to the optimal offset identified earlier. As done by the authors in previous works, different discrete values for the fiber rotation have been tested. In this work the results obtained with 3, 5 and 6 degrees of rotation are shown. It can be seen that the solution with $+5°$ rotation is the best one in terms of mass and load reduction. Remarkably, the integration of flap/edge coupling and BTC allows one to further save mass (-3.31%) and reduce loads, in particular the combined moment at blade root(-5.31%) and the combined nodding-yawing moment at hub (-4.7%). It must be noticed that for each solution the computation of the COE is performed following [4, 10], in order to allow for a direct comparison against previous and ongoing activities within the INNWIND.EU consortium.

Table 4: Integrated offset and BTC against baseline.

	Baseline	Offset 20 cm	Off20 + BTC05
AEP [GWh/yr]	46.126	46.107 (-0.04%)	46.016 (-0.24%)
Blade mass [kg]	42445	40741 (-4.0%)	39461 (-7.0%)
COE [EUR/MWh]	75.637	75.523 (-0.15%)	75.559 (-0.1%)
Blade root comb. mom. [kNm]	72497	71435 (-1.5%)	67642 (-6.7%)
Hub comb. mom. [kNm]	60334	54109 (-10%)	51566 (-14.5%)
Tower top comb. mom. [kNm]	62012	55613 (-10%)	54435 (-13.9%)

Table 4 shows a direct comparison between the integrated solution and the initial baseline, showing a significant reduction of the loads, in particular the maximum combined moment at hub (-14.5%). However, the AEP is slightly reduced, which poses a serious limit to the global impact of the lightweight design on the cost of energy. In fact, although an important mass reduction is achieved (-7.0%), the cost reduction is almost negligible, due to the lower energy production.

3.3. Rotor resizing

In order to turn the beneficial effects of the integrated flap/edge coupling and BTC into significant cost advantages, this study has been completed with a resizing of the rotor swept area. To exploit the load reductions shown earlier, a larger rotor has been designed with the main goal of increasing its energy capture. Thus, starting from the optimal combination of 20 cm spar cap offset and 5° of fiber rotation, the rotor radius has been gradually increased, until a solution of a mass-minimizing optimization problem with the same combined moment at the hub was found. In this way, for each blade length, a new design was obtained that satisfies all constraints.

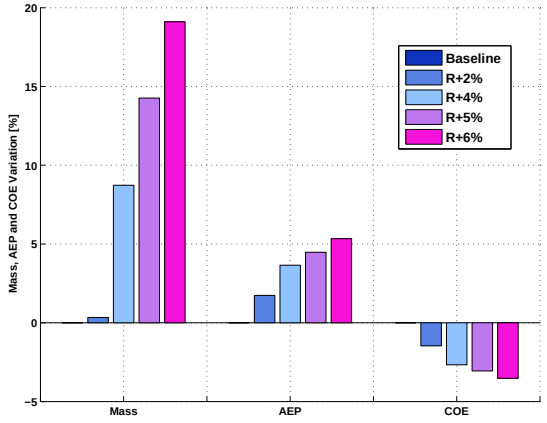

Figure 8: Rotor resizing: mass, AEP and COE.

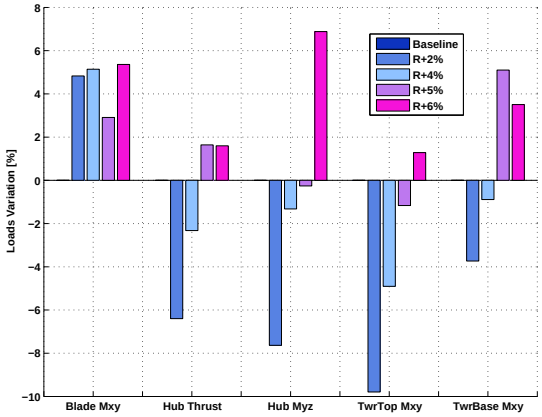

Figure 9: Rotor resizing: ultimate loads.

Figure 8 and 9 illustrate the consequences of the rotor radius increase, in terms of mass, AEP, COE and ultimate key loads. In general, it can be observed that increasing the radius results in larger mass and AEP, and lower COE. Looking at the load diagram, it appears that a radius extension of 5% attains basically the same combined moment in the hub frame as the inial baseline. If the radius is further extended to 6%, all the key loads grow significantly and the constraint of developing the same hub moment as the baseline is violated.

	Baseline	Offset 20 cm	Off20 + BTC05	R + 5%
Blade mass [kg]	42445	40741 (-4.01%)	39710 (-6.44%)	48519 (+14.31%)
AEP [GWh]	46.126	46.107 (-0.04%)	46.079 (-0.1%)	48.191 (+4.48%)
CoE [EUR /MWh]	75.637	75.523 (-0.154%)	75.481 (-0.2%)	73.323 (-3.06%)

Table 5: Summary of the lightweight design process.

Table 5 summarizes the outcomes of the multi-step lightweight design, giving a direct comparison between the initial baseline and the partial and final optimal configurations. The main achievement of this process is a remarkable reduction of the levelized cost of energy. This comes as the consequence of a resized rotor that, although having a larger swept area, develops the same loads in the hub frame. It must be noticed that not all loads have been decreased, and in particular Figure 9 shows that the ultimate combined moment at tower base is increased of about 5%, which can have an impact on the design of the tower segments. However, this variation has been considered as acceptable in the context of this work, where the focus is mainly related

to the blade design. Figure 10 compares the thickness of some structural elements, and one may notice how the final solution with increased radius requires a much thicker spar cap, due to the effect of the active tip displacement constraint.

4. Conclusions

In this work we have investigated the beneficial effects on blade mass and loads of a varying offset between the pressure-side and suction-side spar caps. An optimal offset was identified, and the corresponding solution was further modified by a rotation of the fibers, showing that significant advantages may be obtained by the combination of these two techniques. This lightweight configuration has been exploited in order to increase the rotor swept area, demonstrating that the corresponding increase in AEP can drive down the cost of energy significantly.

It must be noticed that only the blade design was accounted for during this study, and detailed redesigns of hub and tower could possibly follow as part of a more comprehensive investigation. Similarly, detailed buckling analyses should be performed via high-fidelity FEM models for all solutions, in order to capture local effects. Since the baseline blade (with no offset nor fiber orientation) has been designed including detailed FEM analyses, we expect that the solutions presented here should not be significantly altered by a detailed FEM verification, as its loads are almost unchanged. Finally, as part of a comprehensive blade redesign activity, a full aero-structural design will be performed in order to study how the spar cap offset can influence the optimal design of chord, twist and blade thickness.

Acknowledgments

The present work is partially supported at Politecnico di Milano by the European FP7 INNWIND.EU project. The authors thank Prof. P. Weaver and Dr. A. Brinkmeyer of the University of Bristol.

References

[1] Bottasso C L, Campagnolo F, Croce A and Tibaldi C 2012 Optimization-based study of bendtwist coupled rotor blades for passive and integrated passive/active load alleviation *Wind Energy* **16** 1149
[2] Buckney N, Green S, Pirrera A and Weaver P 2013 On the structural topology of wind turbine blades *Wind Energy* **16** 545
[3] Buckney N, Pirrera A, Weaver P and Griffith D T 2014 Structural efficiency analysis of the sandia 100 m wind turbine blade *AIAA Science and Technology Forum and Exposition 2014: 32nd ASME Wind Energy Symposium* (National Harbor)
[4] Lekou C et Al 2015 *INNWIND Deliverable 2.22 New lightweight structural blade designs & blade designs with built-in structural couplings*
[5] Chaviaropoulos P et Al 2015 *Deliverable 1.24, PI-based Assessment of the Results of WP2-WP4 - Ongoing Integration" Action September 2015*
[6] Bottasso C L, Campagnolo F and Croce A 2011 Multi-disciplinary constrained optimization of wind turbines *Multibody Syst. Dyn.* **27** (DOI: 10.1007/s11044-011-9271-x)
[7] Bak C et Al 2013 Description of the DTU 10 MW reference wind turbine, *DTU Wind Energy Report-I-0092* (Roskilde)
[8] Croce A, Sartori L, Lunghini M S and Bottasso C L 2016 Structural design of 10 MW wind turbine rotors *Wind Energy Science* (submitted)
[9] IEC 61400-1:2005 Wind Turbines Part 1: Design Requirements *International Standard IEC 61400-1*
[10] Fingersh L., Hand M., Laxson A.: Wind turbine design cost and scaling model, NREL/TP-500-40566, National Renewable Energy Laboratory, Golden, USA, 2006
[11] Bottasso C L Croce A 2016 *Cp-Lambda a Code for Performance, Loads, Aeroelasticity by Multi-Body Dynamics Analyis*, **Version 6.30**

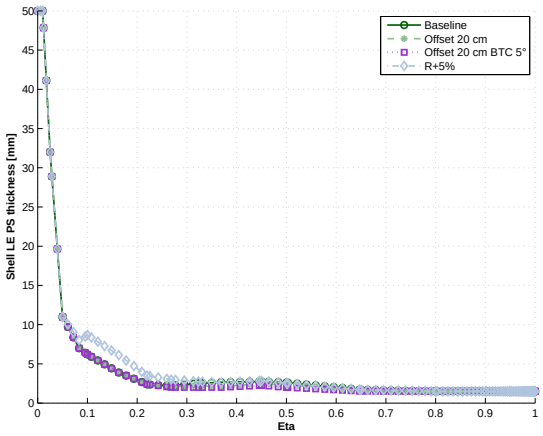

(a) Shell.

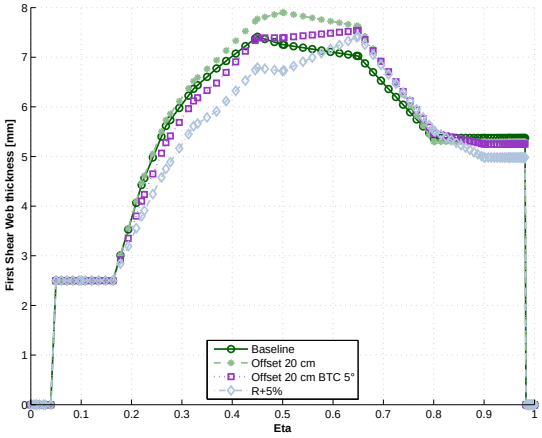

(b) Main webs.

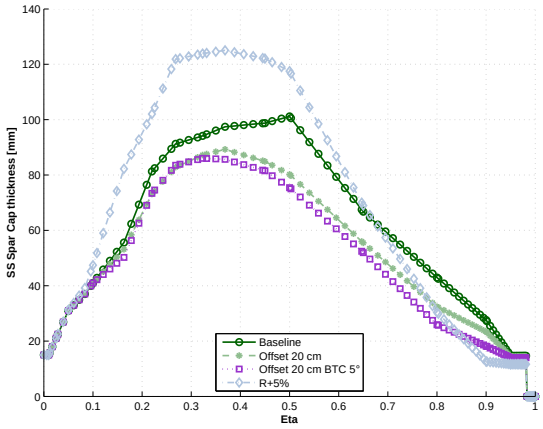

(c) Suction-side spar cap.

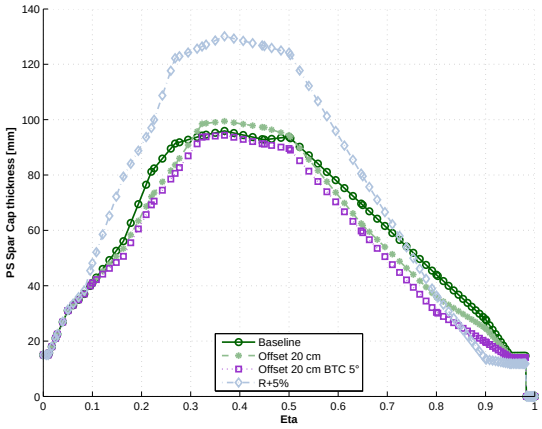

(d) Pressure-side spar cap.

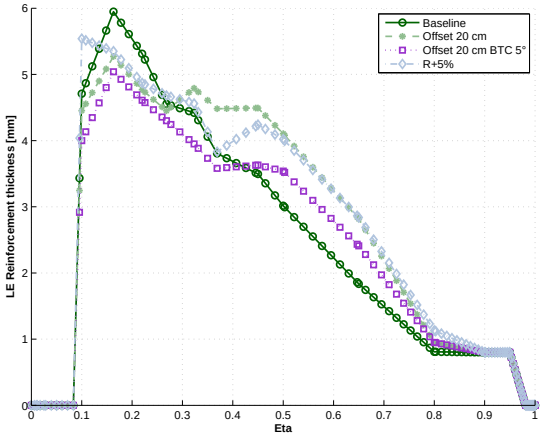

(e) Leading edge reinforcement.

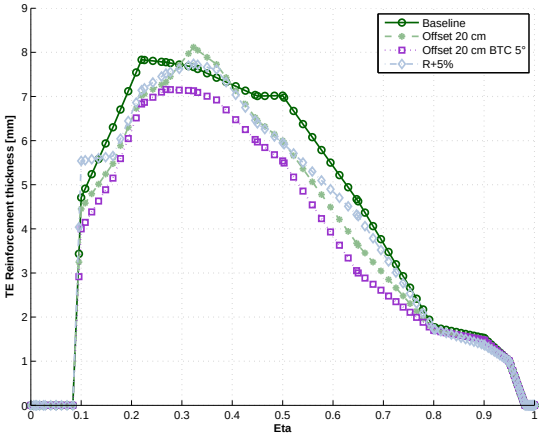

(f) Trailing edge reinforcement.

Figure 10: Span-wise thickness distribution of structural components.